Journal of Physics D: Applied Physics

PAPER • **OPEN ACCESS**

Circular Airy-like beams through leaky-wave antennas

To cite this article: Alessio Benedetti *et al* 2023 *J. Phys. D: Appl. Phys.* **56** 085102

OPEN ACCESS
IOP Publishing
Journal of Physics D: Applied Physics
J. Phys. D: Appl. Phys. **56** (2023) 085102 (7pp)
https://doi.org/10.1088/1361-6463/acb5ab

Circular Airy-like beams through leaky-wave antennas

Alessio Benedetti[1,*], **Davide Comite**[1], **Walter Fuscaldo**[2], **Paolo Baccarelli**[3], **Alessandro Galli**[1] and **Paolo Burghignoli**[1]

[1] Department of Information Engineering, Electronics and Telecommunications, Sapienza University of Rome, Via Eudossiana 18, 00184 Rome, Italy
[2] Consiglio Nazionale delle Ricerche, Istituto per la Microelettronica e Microsistemi (CNR-IMM), Via del Fosso del Cavaliere 100, 00133 Rome, Italy
[3] Department of Industrial, Electronic, and Mechanical Engineering, Roma Tre University, Via Vito Volterra 62, 00146 Rome, Italy

E-mail: alessio.benedetti@uniroma1.it

Received 27 October 2022, revised 6 January 2023
Accepted for publication 24 January 2023
Published 9 February 2023

Abstract

A planar nonuniform radially periodic leaky-wave antenna is proposed for the generation of circular, azimuthally symmetric Airy beams. The design is compact and low cost, and it is excited by an integrated coaxial cable. An annular metal strip grating is considered as background structure, designed to support a fast, backward, radially propagating space harmonic, which is capable of generating nondiffracting fields. The period and slots width are then properly modulated to synthesize the relevant Airy-like aperture-field distribution. An approximate formula is proposed to describe the aperture field, which is then used to retrieve the pattern of the annular strips. The near field produced by the structure is evaluated through the radiation integral, and validated by means of numerical full-wave simulations.

Keywords: leaky-wave, Airy function, holography, microwaves, circular antenna, radial tailoring

(Some figures may appear in colour only in the online journal)

1. Introduction

Airy beams (ABs) have attracted considerable interest thanks to a number of interesting properties [1–6]: they can be weakly diffractive compared to, e.g. Gaussian-like beams, exhibit a self-healing character (as per Bessel beams [7, 8]), and have the ability to abruptly focus their energy towards a point in front of a planar aperture [9–11]. ABs have initially been defined for two-dimensional (2D) propagation [1]. Various realization techniques have been proposed, first in the optical range (e.g. through holographic techniques [12]) and more recently in the microwave range [13–21]. Many developments have been introduced to extend the 2D formulation and realization to a three-dimensional (3D) domain, thus obtaining the so-called circular ABs (CABs) [22–29].

There is broad interest in designing compact and low-cost antenna solutions with novel near-field performance operating in the microwave range, with applications ranging from near-field communications and wireless power transfer to near-field probing, radar imaging, medical imaging. In this work, we propose a novel approach for the generation of CABs at microwaves by means of a *nonuniform radially periodic leaky-wave antenna* (LWA) (see figure 1). The structure consists of a grounded circular dielectric slab covered by an annular strip grating (bull's-eye (BE) LWA), whose presence perturbs the propagation of the relevant surface wave, thus establishing a leaky-wave radiation regime. The strip grating can properly be

* Author to whom any correspondence should be addressed.

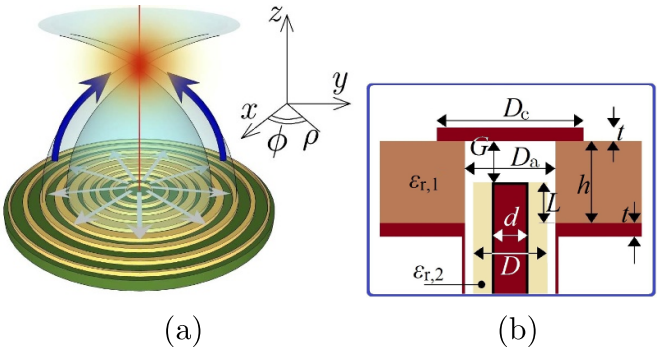

Figure 1. Generation of an Airy-like, abruptly autofocusing beam through a planar, radially periodic bull's eye leaky-wave antenna. (a) A cylindrical wave (white arrows) is excited from the source and converted by the *nonuniform* annular strip grating into a backward cylindrical leaky mode that radiates most of its energy in a focused spot (reddish region) following the typical accelerated trajectories (blue arrows) of Airy beams. (b) Detail of the coaxial-based feeder. *Parameters*: $h = 3.14$ mm, $\varepsilon_{r,1} = 2.2$, $d = 0.31$ mm, $D = 0.99$ mm, $D_a = D + 0.1$ mm, $\varepsilon_{r,2} = 2.1$, $G = 0.24$ mm, $L = 2.9$ mm, $D_c = 10$ mm, $t = 35\ \mu$m.

designed to support *backward cylindrical leaky waves*, which may profitably be used to radiate *conical beams* in the far field [30] or *nondiffracting beams* (e.g. Bessel beams) in the near field [31]. Here, the leaky-wave approach is originally applied to the generation of an Airy-like beam, by introducing a modulation of *both periods* and *strip widths* of the radially periodic LWA, which is therefore nonuniform. The dispersion properties of the unit cell for different values of the geometrical parameters have been obtained with accurate numerical simulations to create a mapping between the relevant complex leaky wavenumber and the available design parameters. This mapping is then used to synthesize the aperture distribution needed to generate the desired Airy-like profile, on the basis of the synthesis formulas for cylindrical leaky waves presented in [32].

The paper is organized as follows. In section 2, we introduce the theory of CABs. In section 3, the design of BE-LWAs generating CABs is presented. Numerical results that validate the design process are provided in section 4, and conclusions are drawn in section 5.

2. Cylindrical ABs

Let us first consider *scalar* beams. By introducing cylindrical coordinates (ρ, ϕ, z), we add the cylindrical spreading factor $1/\sqrt{\rho}$ to the field of a standard 2D AB (see, e.g. [2]), thus obtaining the following azimuthally invariant aperture distribution

$$\begin{aligned} \mathrm{U}_{3\mathrm{D}}(\rho) = \frac{1}{\sqrt{\rho}}\mathrm{Ai}\left[b\left(\rho-\rho_0-\frac{b^3}{4k_0^2}z_\mathrm{E}^2\right)-\mathrm{j}\frac{ab}{k_0}z_\mathrm{E}\right] \\ \cdot\exp\left\{-a\left(\rho-\frac{b^3}{2k_0^2}z_\mathrm{E}^2\right)\right. \\ \left.+\mathrm{j}\left\{\frac{z_\mathrm{E}}{2k_0}\left[a^2-b^2(\rho-\rho_0)\right]-\frac{b^6}{12k_0^3}z_\mathrm{E}^3\right\}\right\} \quad (1) \end{aligned}$$

where k_0 is the vacuum wavenumber; ρ_0 defines the boundary between the evanescent and oscillating parts of the aperture distribution; $z_\mathrm{E} > 0$ is the abscissa of the aperture plane; $a > 0$ is the decay rate of the exponential function that guarantees the square integrability of the aperture field; and $b < 0$ establishes an inward acceleration of the radiated field. It can be shown that the Fourier–Bessel spectrum of (1) shows high similarities with the Fourier spectrum of the aperture distributions of standard 2D ABs. A similar behavior of the radiated near field is thus expected.

Let us now consider *vector* beams. For simplicity, only azimuthally invariant transverse magnetic (TM) fields are considered, which can be excited by feeding the antenna with an azimuthally symmetric source such as, e.g. a centered vertical coaxial probe [30, 31, 33].

As a first, preliminary remark, we observe that the only nonzero components of the considered TM azimuthally invariant fields are E_ρ, E_z, and H_ϕ and that, in principle, a CAB profile could be associated with any of them. However, the paraxial (hence, quasi-TEM) character of ABs suggests to keep the E_z component of the aperture field as small as possible. Therefore, the synthesis will be based on a tangential component of the aperture field; in particular, we will enforce a CAB profile on the component H_ϕ.

Furthermore, as discussed in [33], it is necessary to select an emission (or aperture) plane $z = z_\mathrm{E} \neq 0$ to synthesize the desired CAB profile. In fact, all Airy-related beams are real on the $z = 0$ plane, with the local phase thus being piecewise constant and assuming integer multiples of π. This condition would lead to the design of an LWA working inside the *open stopband* [34], thus preventing from the correct tailoring of the profile of the attenuation constant (i.e. α) of the leaky mode by using a simple single strip geometry inside the unit cell.

Having said that, the synthesis of the desired CAB profile for $H_\phi(\rho, z = z_\mathrm{E})$ is achieved by assuming that the field on the emission plane is dominated by a cylindrical leaky wave with a nonuniform radial wavenumber $k_\mathrm{LW}(\rho) = \beta(\rho) - j\alpha(\rho)$. The radial dependence of such a wavenumber can be determined by using the design formulas for 2D LWAs derived in [32] and used for the synthesis of Bessel–Gauss beams in [31, 33].

To illustrate the procedure and as a first reference example, we consider the case of a CAB profile for H_ϕ given by (1) with $b = -80\ \mathrm{m}^{-1}$, $\rho_0 = 6\lambda_0$, $a/k_0 = 0.04$, and $z_\mathrm{E} = 2\lambda_0$, over a radiative region of depth along z equal to $15\lambda_0$.

In agreement with the study reported in [35], we observed a peculiar behavior when inspecting all CAB functions at $z \geqslant 0$: the complex field values present a decreasing phase profile in a radial zone extending from the center (i.e. at $\rho = 0$) to a point approximately located at the end of the first emitting lobe (marked with a red '+' and a magenta vertical dashed line respectively in figure 2(b)); this first and inner radial section is representative of a continuous backward emission. Beyond this point, which we shall refer to as the flipping behavior point, the phase assumes a staircase-like behavior; however, the Airy emission still preserves its backward emission character.

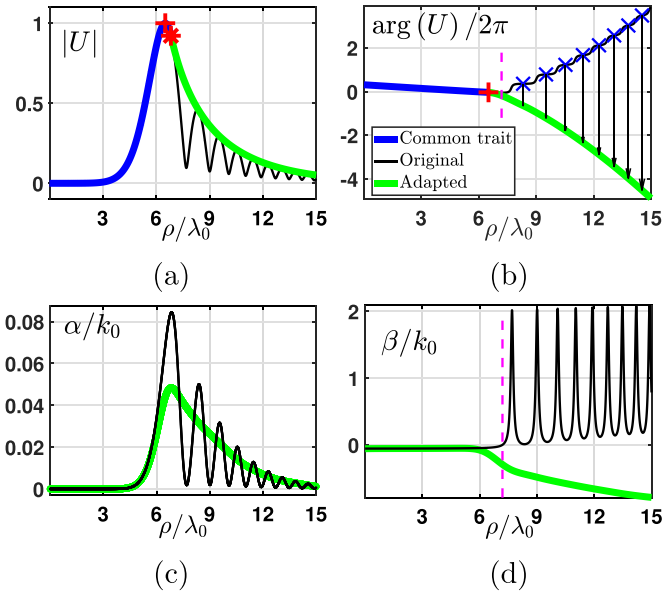

Figure 2. (a) and (b): Absolute value and normalized phase of the original and adapted radial field profiles for CAB emission; the red '+' and '*' refer to the U norm peak value and the outermost point of the common trait, respectively. The phase $\arg(U)$ decreases until reaches a minimum, indicated with a red '+'; in (b), several blue crosses indicate the spots where the outer lobes emission takes place, falling across the local minima of the original phase constant profile shown in (c); by lowering them of an integer number of 2π, we get the adapted Φ profile plotted with a thick green line. (c) and (d): The relevant radial profiles of the normalized attenuation and phase constants. *Parameters*: $f_0 = 18$ GHz, $b = -80\,\mathrm{m}^{-1}$, $\rho_0 = 6\lambda_0$, $a/k_0 = 0.04$, $z_\mathrm{E} = 2\lambda_0$.

This last feature could seem contradictory, but it is made possible by the simultaneous presence of an oscillating amplitude and suitable phase differences between points corresponding to the oscillating amplitude peaks (see the red cross in figure 2(b)). These two features combined together promote an array-like emission with an *effective* homogeneous backward character, despite the resulting β function being affected by strong oscillations (due to the phase jump discontinuities) and progressively assuming positive values at higher radial positions (see figure 2(d)). The different radiating configuration between these two distinct zones explains why there is always a remarkable difference in terms of power between the innermost CAB lobe and the outer lobes. The same and opposite phenomenon takes place at $z \leqslant 0$, with forward emission replacing the backward one.

We took advantage of this observation by joining the first smooth portion of the original phase function, roughly extending from $\rho = 0$ until the maximum value of the CAB absolute value (indicated with a red cross in figure 2(a)), with the subsequent discrete set after subtracting progressively increasing integer multiples of π. Then, we interpolated the entire set of values to finally get, via derivation, the smooth continuous β function. This *adapted* β variant presents no oscillations, as shown with a thick green line in figure 2(d). In a similar fashion, we suppressed the amplitude oscillations by replacing the original Airy $\mathrm{Ai}(\cdot)$ function with a proper combination of this latter with the corresponding Airy $\mathrm{Bi}(\cdot)$ function [36] in the radial region located beyond the peak of $|U|$. The resulting β explains why, as opposed to the case of radiation of Bessel and Bessel–Gauss beams, CABs require a strongly variable emission angle along the radial direction (which in turn will require a variable local periodicity of the BE metal slots). This feature of CABs, however, allows for generating a nondiffracting wave mainly focused on a spot in front of the aperture, in contrast with the nondiffracting beam typical of monochromatic Bessel-like solutions.

The resulting α profile is shown in figure 2(c), with thick green and thin black lines representing the α profile of the adapted and original CAB functions, respectively. Also in this case, oscillations are suppressed in the adapted profile.

A careful analysis of the near fields produced by the exact and adapted aperture distributions shows that a good agreement can be found provided the abscissa of the emission plane z_E is not too large; a practical value is $z_\mathrm{E} = 2\lambda_0$. It is worth noting that the adapted profile induces a stronger radiation from secondary lobes, and this in turn produces a small but observable lowering and enhancement of the near-field focus. This is clearly advantageous, because achieving a hot spot in tight proximity of the radiating structure is usually considered a challenging task.

3. Antenna design

As a reference structure we consider the grounded dielectric slab used in [31], i.e. a laminate Taconic TLY-5 with relative permittivity 2.2, loss tangent 9×10^{-4}, and substrate thickness 3.14 mm.

As already mentioned, a focused beam can be obtained by using BE-LWAs provided that the grating parameters Λ (period) and W (strip width) are suitably designed to support a *backward* leaky wave, i.e. a leaky wave with $\beta < 0$ [37]. A reference frequency is here set at $f_0 = 18$ GHz and the focusing features of the antenna will be analyzed within a larger bandwidth. The normalized phase and attenuation constants β/k_0 and α/k_0 of the operating TM leaky mode supported by the linearized BE are reported in figure 3 with colormaps in the (FF, Λ) plane, where $\mathrm{FF} = W/\Lambda$ is the filling factor, Λ is the radial period, and W is the strip width of the linearized BE.

To perform the CAB-radiating BE-LWA design stage, we proceeded as done for the synthesis of a BE-LWA radiating Bessel, Gauss and Bessel–Gauss beams [33], having now to deal with the additional feature of a variable radial period in order to accommodate a radially varying β. In particular, we selected a continuous set of (Λ, FF) pairs which best matched all points of the curves in figures 2(c) and (d) (see green thick lines). The (Λ, FF) linear profiles were extracted from the data shown in figure 3 (the algorithm used for the search prevents sudden jumps from too distant value sets in order to avoid design discontinuities between adjacent unit cells). By setting an inner radial spot $\rho_{\mathrm{c},0}$ and using

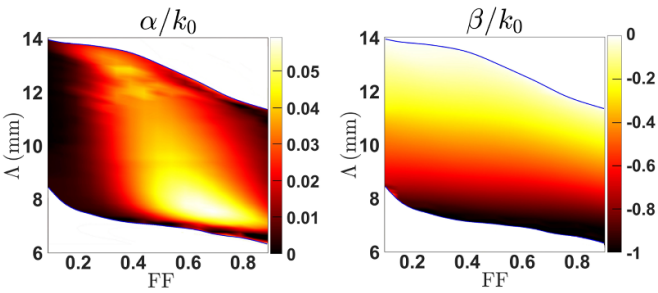

Figure 3. Colormaps for the normalized leakage constant α/k_0 (left) and the normalized phase constant β/k_0 (right) in the (FF, Λ) plane (where FF $= W/\Lambda$ is the filling factor, Λ is the radial period, and W is the strip width of the linearized BE), evaluated for a Taconic TLY-5 substrate with relative permittivity 2.2, loss tangent 9×10^{-4}, and thickness 3.14 mm, at $f = 18$ GHz. The blue line indicates the boundary between negative and positive values of β (the latter are not useful for our design and are not reported).

iterative expressions, we finally extracted a discrete set of (ρ_c, W) values to design the metal strip sequence, with ρ_c and W respectively referring to the central position and the horizontal width of each metal strip: $\rho_{c,0} \rightarrow \rho_{c,k+1} = \rho_{c,k} + [\Lambda(\rho_k) + \Lambda(\rho_{k+1})]/2$, $W_k = \Lambda(\rho_{c,k}) \cdot \mathrm{FF}_k(\rho_{c,k})$.

Caution should be taken when choosing a design configuration. In fact, one including a high α/k_0 peak value could not be sufficiently emulated by a BE-LWA design with the available dataset. For the same reasons, a slope too high could be difficult to reproduce with the proposed technology, since it would require a distance shorter than the spacing values Λ of our dataset; moreover, even when attainable with a BE-LWA design, a high slope usually induces backscattering and the consequent formation of internal resonant counter-propagating cylindrical waves, which could introduce unbearable complexities in the same design process. For this reason, it is convenient to choose contained values for $|b|$ and sufficiently large values for r.

4. Numerical results

In order to validate the proposed design strategy, in this section full-wave simulations are reported for a specific structure. In particular, CST Microwave Studio [38] and Ansys Lumerical [39] have been used to calculate the aperture field over the LWA aperture plane; subsequently, the near-field distribution has been calculated in Matlab [40] by evaluating the Stratton–Chu radiation integrals [41].

The design assumed a CAB aperture distribution characterized by the parameters $\eta_I = 0.9$, $\rho_0 = 6\lambda_0$, $\mathrm{r} = 15\lambda_0$, $b = -80$ m^{-1}, $z_E = 2\lambda_0$, and $a = 0.04k_0$. The resulting α/k_0-peak and slope are 0.048 and 0.0247, respectively, with an Airy front extent of 3 cm, indicating that a BE-LWA design is possible with the available geometrical ranges of the metal strips. The width and radial positions of the strips resulting from the synthesis are reported in table 1. The antenna is fed by a vertical coaxial probe placed below a central metal disk whose radius and distance from the probe have been optimized to achieve

Table 1. Width W_k and radial position $\rho_{c,k}$ ($k = 1, \ldots, 20$) expressed in (mm) for each metal strip of the designed BE-LWA.

k	1	2	3	4	5	6	7	8	9	10
W_k	1.4	1.6	2.3	3.5	5.3	5.3	4.5	3.8	3.5	3.2
$\rho_{c,k}$	57	71	84	97	109	120	131	141	150	160
k	11	12	13	14	15	16	17	18	10	20
W_k	2.9	2.6	2.4	2.2	2	1.7	1.3	1	1	1
$\rho_{c,k}$	169	178	187	196	205	214	222	231	239	248

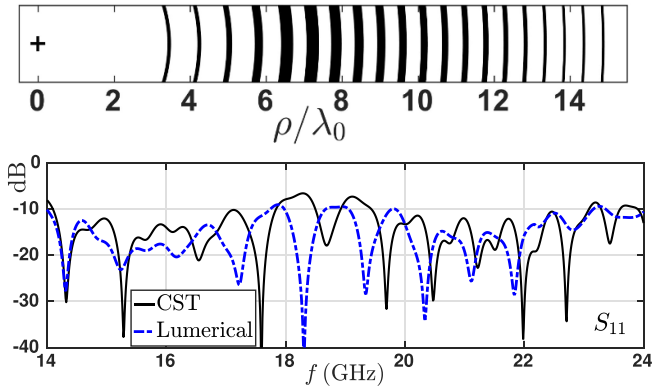

Figure 4. (Top) Top-view portion of BE-LWA annular pattern with strip widths and radial positions as in table 1, and (bottom) the relevant input reflection coefficient S_{11} in absolute value (in dB) as a function of frequency, evaluated with CST (black solid line) and Lumerical (blue dotted-dashed line).

good input matching (the relevant geometrical parameters are given in [31]).

In figure 4(a) a portion of the resulting BE-LWA annular metal pattern is reported. The relevant input reflection coefficient evaluated with CST and Lumerical is reported in figure 4(b) in absolute value (in dB) as a function of frequency; it shows that a good input matching has been achieved around the operating frequency at 18 GHz.

In figures 5(a) and (b) the normalized phase and attenuation constants β/k_0 and α/k_0 of the adapted CAB function and of the final synthesized BE-LWA are compared. The modifications introduced to accommodate the design process with BE-LWA technology appear to be quite efficient despite the presence of some limited differences, mainly traceable to the now stronger outer Airy lobes of the adapted function.

This also explains the small supplementary lowering and sharpening of the hot spot region (HSR) along the z-axis, which can be observed in the near-field distributions reported in the second and third columns of figure 6 (obtained by numerically evaluating the Stratton–Chu radiation integrals in Matlab and by performing full-wave simulations in CST, respectively) with respect to the distribution produced by evaluating the Stratton–Chu radiation integrals starting from the original CAB aperture field, reported in the first column of the same figure. The small field perturbation observed in a narrow region around the central vertical axis below the HSR is mainly due to resonant reflections occurring inside the BE-LWA in a

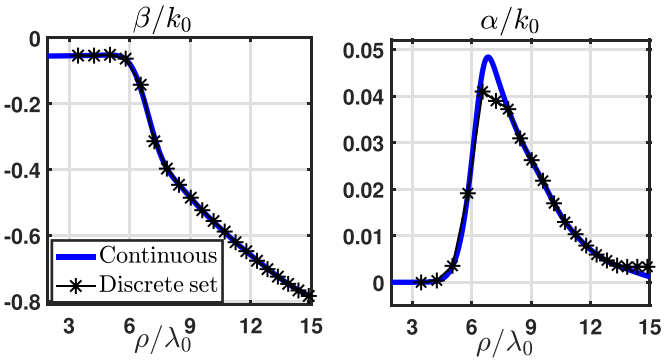

Figure 5. (Left inset) α/k_0 and (right inset) β/k_0 radial profiles of the adapted CAB function (blue solid line) and of the final synthesized BE-LWA (black thin line with asterisks). CAB parameters: $\rho_0 = 6\lambda_0$, $\mathrm{r} = 15\lambda_0$, $b = -80\ \mathrm{m}^{-1}$, $a/k_0 = 0.04$, $z_\mathrm{E} = 2\lambda_0$.

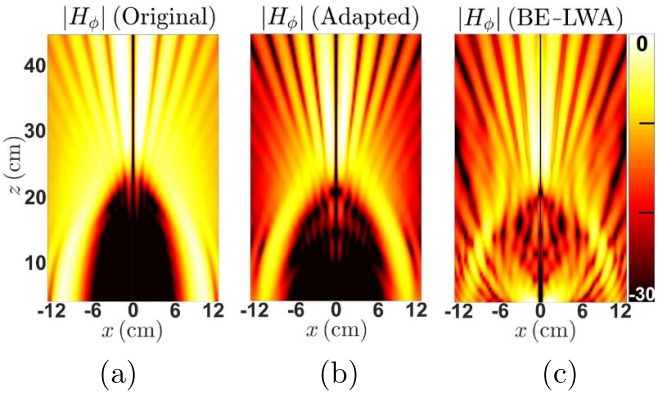

Figure 6. Near-field distributions of H_ϕ (in absolute value and in dB) produced by the original CAB aperture field radiating from $z_\mathrm{E} = 0$ (left)), by its adapted variant radiating from $z_\mathrm{E} = 2\lambda_0$ (center), and radiated by the BE-LWA shown in figure 5(c) (right). (a) and (b) have been obtained by means of a numerical evaluation of Stratton–Chu radiation integrals in Matlab, whilst (c) has been obtained by CST. The normalization factor was set to the maximum value of E_z norm across the focus divided by the vacuum impedance ζ_0.

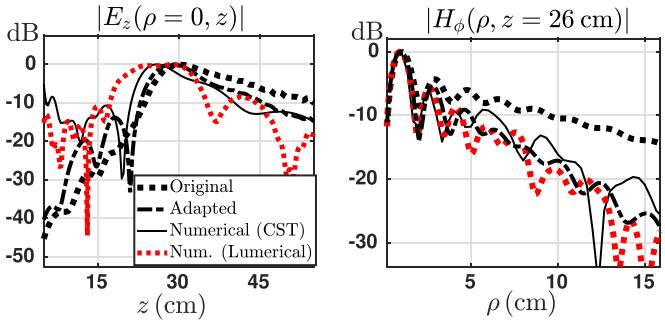

Figure 7. Normalized field profiles in absolute value (in dB) for the structure of figure (5) at $f = 18$ GHz: comparison between theoretical results (original and adapted) and 3D numerical simulations (CST and Lumerical). (Left) E_z along z at $\rho = 0$; (Right) H_ϕ along ρ at $z = 26$ cm.

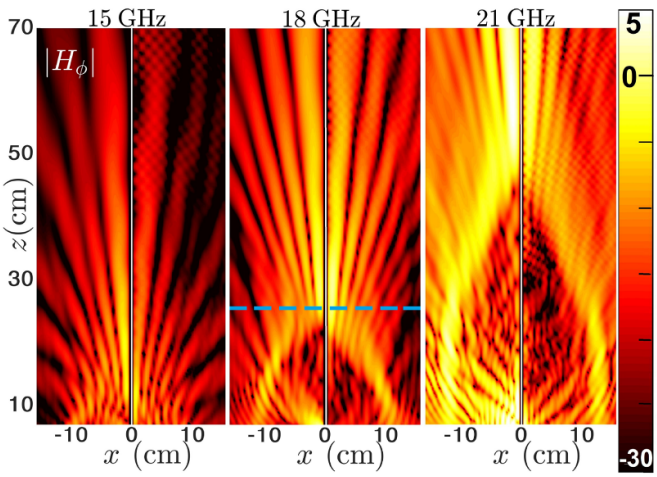

Figure 8. Normalized H_ϕ norm distributions calculated at $f = 15$, 18 and 21 GHz for the structure of figure (5). Each subfigure is split in two halves, left (CST) and right (Lumerical). The cyan dashed line in the center figure indicates the abscissa $z = 26$ cm.

region approximately defined by the α/k_0 peak; interactions with the internal disk, which has been introduced at the center in order to achieve a good impedance matching at the input coaxial port (see [31]), also induce these spurious patterns. Note that the $|E_z|$ peak value is 2.5 times higher in the adapted configuration than the respective value in the original one, with a power ratio close to 6.

Figure 7 reports longitudinal and transverse field profiles for E_z and H_ϕ, respectively. In general, a good agreement has been achieved among the theoretical case and the nonuniform LWA implementation proposed in this work.

By varying the operating frequency, according to the inherently dispersive features of the background leaky mode supported by the linearized BE-LWA (see [31], where the phase and attenuation constants of a leaky mode supported by this class of structure is reported) the near-field distribution of the antenna will change; therefore, the focus of the Airy-like beam will be modulated. Figure 8 reports the field maps for two additional frequencies (i.e. 15 and 21 GHz), compared again with that at $f = 18$ GHz. As expected, based on a simple ray-optics approximation [31, 33], higher frequencies generate acceleration that focuses the beam farther away from the antenna aperture. The same behavior can be observed for all the three components of the radiated field reported in figure 8. Figure 9 reports longitudinal and radial cuts for the same frequencies as in figure 8. The aforementioned shift of the focus is clearly visible in the longitudinal cut, whereas the transverse behavior remains fairly consistent at the three considered frequencies. Note that, in the shown frequency range, the total efficiency of the antenna calculated with CST, defined as the ratio between the radiated power and the incident power at the input port, attains values between 80 and 90%.

Finally, a synthetic figure of merit (FoM) can be introduced in order to quantify the frequency variation of the CAB focusing features, as the ratio between the squared electric field averaged both in time over a period and in space over the HSR ($\bar{\mathcal{E}}_z^2$) and the real power emitted by the antenna aperture (P_R):

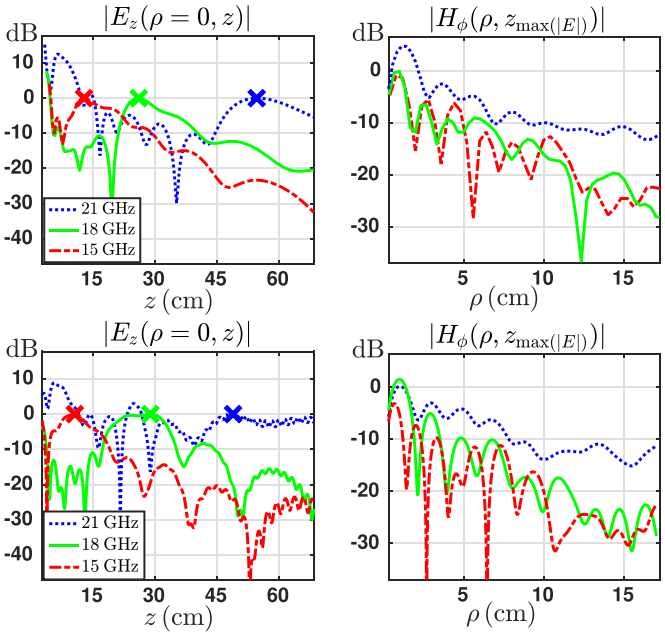

Figure 9. Same as in figure 7, calculated by 3D simulations at 3 different frequencies (21, 18 and 15 GHz) with CST (top row) and Lumerical (bottom row). The thick crosses in the leftmost insets indicate the position of the $|E_z|$ peak.

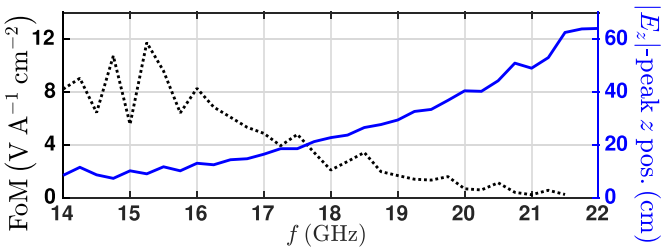

Figure 10. Focusing figure of merit (FoM, defined in (2)) and position of the peak of $|E_z|$ along the z-axis as a function of frequency, for the BE-LWAs of figure 5.

$$\mathrm{FoM} = \frac{\bar{\mathcal{E}}_z^2}{P_\mathrm{R}}. \tag{2}$$

Such a FoM is reported in figure 10 (left axis) in a frequency range from 14 to 22 GHz together with the position of the peak of $|E_z|$, i.e. of the near-field focus (right axis). The trend is clearly decreasing with frequency; the oscillations at lower frequencies are due to the difficulty of defining clearly the HSR when it is very close to the antenna aperture.

5. Conclusions

The realization of abruptly autofocusing microwave Airy-like beams has been shown to be possible by employing planar radially nonuniform LWA, characterized by a compact geometry and based on commercial printed elements with a simple coaxial feed.

A cylindrical, azimuthally symmetric, version of the classical AB has been derived and validated. By suitably adapting its radial field profile, the synthesis of the beam has been achieved by means of a radial tapering of the geometrical parameters of the BE antenna.

Numerical full-wave results have validated the effectiveness of the proposed design strategy, confirming the possibility of achieving focused spots in front of the antenna aperture supported by an accelerating beam, modulating its distance by simple changing the frequency. Possible extensions of the present work may consist in employing circular phased arrays of sources in order to create autofocusing beams with higher azimuthal order and hence nonzero orbital angular momentum.

Data availability statement

The data that support the findings of this study are available upon reasonable request from the authors.

ORCID iDs

Alessio Benedetti https://orcid.org/0000-0002-8223-9247
Davide Comite https://orcid.org/0000-0002-5080-3966
Walter Fuscaldo https://orcid.org/0000-0002-0773-6286
Paolo Baccarelli https://orcid.org/0000-0002-4660-0103
Alessandro Galli https://orcid.org/0000-0002-5827-160X
Paolo Burghignoli https://orcid.org/0000-0001-5896-4732

References

[1] Berry M V and Balazs N L 1979 *Am. J. Phys.* **47** 264–7
[2] Siviloglou G A and Christodoulides D N 2007 *Opt. Lett.* **32** 979–81
[3] Siviloglou G A, Broky J, Dogariu A and Christodoulides D N 2007 *Phys. Rev. Lett.* **99** 213901
[4] Bandres M A 2009 *Opt. Lett.* **34** 3791–3
[5] Efremidis N K and Christodoulides D N 2010 *Opt. Lett.* **35** 4045–7
[6] Efremidis N K, Chen Z, Segev M and Christodoulides D N 2019 *Optica* **6** 686–701
[7] Ettorre M, Pavone S C, Casaletti M, Albani M, Mazzinghi A and Freni A 2018 Near-field focusing by non-diffracting Bessel beams *Aperture Antennas for Millimeter and Sub-Millimeter Wave Applications* ed A Boriskin and R Sauleau (Cham: Springer) pp 243–88
[8] Comite D, Fuscaldo W, Burghignoli P, Galli A and Baccarelli P 2021 Bessel-beam antennas *Wiley Encyclopedia of Electrical and Electronics Engineering* ed J Webster (New York: Wiley) pp 1–12
[9] Anguiano-Morales M, Martínez A, Iturbe-Castillo M D, Chávez-Cerda S and Alcalá-Ochoa N 2007 *Appl. Opt.* **46** 8284
[10] Lu W, Sun X, Chen H, Liu S and Lin Z 2019 *Phys. Rev.* A **99** 1–9
[11] Jiang Y, Zhao S, Yu W and Zhu X 2011 *J. Opt. Soc. Am.* A **35** 890–4
[12] Davis J A, Cottrell D M and Sand D 2012 *Opt. Express* **20** 13302–10
[13] Hao W, Deng M, Chen S and Chen L 2019 *Phys. Rev. Appl.* **11** 054012

[14] Feng R, Ratni B, Yi J, Zhang K, Ding X, Zhang H, Piau G P, de Lustrac A and Burokur S N 2020 *Phys. Rev. Appl.* **14** 014081
[15] Huang Y, Li J, Xu H X, Yu H, Yang Z, Yu P, Hu W, Inserra D and Wen G 2020 *IEEE Trans. Antennas Propag.* **68** 7507–16
[16] Miao Z-W and Hao Z-C 2020 Generation of millimeter-wave and terahertz airy waves using metasurfaces *2020 13th UK-Europe-China Worksh. Millim.-Wav. THz Techn. (UCMMT) (Tianjin, China, 29 August–1 September 2020)* pp 1–3
[17] Feng R, Ratni B, Yi J, Zhang H, de Lustrac A and Burokur S N 2021 *Photon. Res.* **9** 1650–9
[18] Fang Z, Chen R, Ryou A and Majumdar A 2021 *ACS Photonics* **8** 2139–47
[19] Yang Z, Wen G, Hu W, Inserra D, Huang Y and Li J 2020 *IEEE Trans. Antennas Propag.* **69** 2290–301
[20] Li H, Hao W, Yin X, Chen S and Chen L 2019 *Adv. Opt. Mater.* **7** 1900493
[21] Cicchetti R, Faraone A and Testa O 2019 *IEEE Access* **7** 62184–97
[22] Efremidis N K and Christodoulides D N 2010 *Opt. Lett.* **35** 4045–7
[23] Papazoglou D G, Efremidis N K, Christodoulides D N and Tzortzakis S 2011 *Opt. Lett.* **36** 1842–4
[24] Chremmos I, Efremidis N K and Christodoulides D N 2011 *Opt. Lett.* **36** 1890–2
[25] Chremmos I D, Chen Z, Christodoulides D N and Efremidis N K 2011 *Phys. Rev.* A **85** 1842–4
[26] He J, Wang S, Xie Z, Ye J, Wang X, Kan Q and Zhang Y 2016 *Opt. Lett.* **41** 2787–90
[27] Liu C, Liu J, Niu L, Wei X, Wang K and Yang Z 2017 *Sci. Rep.* **7** 1–8
[28] Huang Y, Li X, Akram Z, Zhu H and Qi Z 2021 *IEEE Antennas Wirel. Propag. Lett.* **20** 1093–7
[29] Kadlimatti R and Parimi P V 2018 *IEEE Trans. Antennas Propag.* **67** 260–9
[30] Comite D, Gómez-Guillamón Buendía V, Podilchak S K, Di Ruscio D, Baccarelli P, Burghignoli P and Galli A 2018 *IEEE Antennas Wirel. Propag. Lett.* **17** 1837–41
[31] Comite D, Fuscaldo W, Podilchak S K, Hílario-Re P D, Gómez-Guillamón Buendía V, Burghignoli P, Baccarelli P and Galli A 2018 *IEEE Trans. Antennas Propag.* **66** 2828–43
[32] Gómez-Tornero J-L, Blanco D, Rajo-Iglesias E and Llombart N 2013 *IEEE Trans. Antennas Propag.* **61** 3475–85
[33] Fuscaldo W, Benedetti A, Comite D, Baccarelli P, Burghignoli P and Galli A 2020 *Phys. Rev. Appl.* **13** 064040
[34] Baccarelli P, Burghignoli P, Comite D, Fuscaldo W and Galli A 2019 *IEEE Antennas Wirel. Propag. Lett.* **18** 2066–70
[35] Kaganovsky Y and Heyman E 2010 *Opt. Express* **18** 8440–52
[36] Vallée O and Soares M 2004 *Airy Functions and Applications to Physics* (Singapore: World Scientific)
[37] Oliner A A and Jackson D R 2007 Leaky-wave antennas *Antenna Engineering Handbook* ed J L Volakis (New York: McGraw-Hill) ch 11
[38] (available at: www.3ds.com/products-services/simulia/products/cst-studio-suite/)
[39] (available at: www.lumerical.com/)
[40] (available at: https://mathworks.com/products/matlab.html)
[41] Stratton J A and Chu L J 1939 *Phys. Rev.* **56** 1